School of Natural Sciences and Mathematics
William B. Hanson Center for Space Sciences

Sequentially Bridged Graphene Sheets with High Strength, Toughness, and Electrical Conductivity—Supplement

UT Dallas Author(s):

Jiuke Mu
Ali E. Aliev
Shaoli Fang
Ray H. Baughman

Citation:

Wan, S., Y. Li, J. Mu, A. E. Aliev, et al. 2018. "Sequentially bridged graphene sheets with high strength, toughness, and electrical conductivity." Proceedings of the National Academy of Sciences of the United States of America 115(21): 5359-5364, doi:10.1073/pnas.1719111115

Supporting Information

Sequentially bridged graphene sheets with high strength, toughness, and electrical conductivity

Sijie Wan[a,b,1], Yuchen Li[a,b,1], Jiuke Mu[c,1], Ali E. Aliev[c], Shaoli Fang[c], Nicholas A. Kotov[b,d,e], Lei Jiang[a,b], Qunfeng Cheng[a,b,2], Ray H. Baughman[c,2]

[a] Key Laboratory of Bio-inspired Smart Interfacial Science and Technology of Ministry of Education, School of Chemistry, Beihang University, Beijing 100191, P. R. China
[b] Beijing Advanced Innovation Center for Biomedical Engineering, Beihang University, Beijing 100191, P. R. China
[c] Alan G. MacDiarmid NanoTech Institute, University of Texas at Dallas, Richardson, TX 75080, USA
[d] Department of Chemical Engineering, University of Michigan, Ann Arbor, Michigan 48109, USA
[e] Biointerface Institute, University of Michigan, Ann Arbor, MI, 48109; USA

[1]S.W., Y.L., and J.M. contributed equally to this work.

[2]To whom correspondence should be addressed. Email: cheng@buaa.edu.cn or ray.baughman@utdallas.edu.

Materials and Methods

Fabrication of G-PCO, πBG, SBG sheets. The as-prepared GO was dispersed in DIW, to realize a concentration of 2 mg·mL^{-1}, by continual stirring for 2 h and ultrasonication for 15 min. Then, 7-8 mL of GO dispersion was filtered under vacuum to make a freestanding GO sheet. After drying at 45 ºC for 24 h, the GO sheet was soaked into pre-mixed THF/PCO solution (3 mg·mL^{-1}) for 1 h, followed by UV irradiation at a wavelength of 254 nm for 2 h in N_2 atmosphere to form a GO-PCO sheet. Subsequently, the GO-PCO sheet was reduced to a G-PCO sheet by immersion in HI solution for 6 h, followed by washing five times with ethanol and drying at 45 ºC for 2 h. Next, the G-PCO sheet was immersed into a pre-mixed DMF/PSE solution (24 mmol·L^{-1}) to absorb PSE molecules, followed by rinsing five times with DMF and drying at 45 ºC for 2 h. Finally, the SBG sheet was obtained by immersing into a pre-mixed DMF/AP solution (24 mmol·L^{-1}) to absorb AP molecules, which can react with PSE molecules by nucleophilic acyl substitution of primary amine group, followed by rinsing five times with DMF and drying at 45 ºC for 2 h. Based on the immersion time in AP and PSE solutions, five kinds of SBG sheets have been fabricated as follows: SBG-I (3 h), SBG-II (6 h), SBG-III (12 h), SBG-IV (24 h), and SBG-V (48 h). The corresponding πBG sheets were fabricated by eliminating treatment with PCO.

Characterization. Atomic force microscopy (AFM) images of GO nanosheets were obtained using a Leica TCS SP5 in the contact mode. Stress-strain curves were measured using a Shimadzu AGS-X Tester at a loading rate of 1 mm·min^{-1}. A conventional frame-mounting method was used for mounting samples for stress-strain measurements. In our application of this method, the sample was adhesively attached to a paper frame that has a rectangular hole cut that is sufficiently wide and long to accommodate the samples width and gauge length. The sample length, gauge length, and width were 10, 5, and 3 mm, respectively. This rigid frame enabled the attachment of the sample to the testing apparatus without damage, and the subsequent cutting of the legs of the frame to release the sample for tensile tests. Fracture rarely occurred near the clamps. The thickness of each tested sample strip was obtained by averaging thickness values at 3 to 5 different positions, which was used to calculate the mechanical property of the corresponding sample strip. Then the average mechanical property for each sample type, and their standard deviations, were obtained from measured property values for 3 to 5 sample strips. To avoid uncertainties in the measurement of sample cross-sectional area, gravimetric strengths were obtained as the ratio of force at break to the sample weight per sample length. Dynamic tensile fatigue tests were conducted at a frequency of 1 Hz using an Instron ElectroPulsE1000 mechanical apparatus and a ratio of the minimum stress to maximum stress of 0.1. The samples used for fatigue testing were 25-mm-long, 5-mm-wide strips. TGA curves were recorded under nitrogen atmosphere on a TG/DTA6300 (NSK, Japan) using a temperature increase rate of 10 ºC·min^{-1} from room temperature to 800 ºC. SEM images were

obtained by field-emission scanning electron microscopy (JEOL-7500F) at an acceleration voltage of 5 kV. Raman spectra were recorded on a LabRAM HR800 (Horiba Jobin Yvon) using 633 nm excitation. The laser power was kept below 0.5 mW to avoid laser heating. For the Raman mapping over a 400 μm^2 square area under different applied strains, Raman spectra were recorded with the step size of 500 nm. All G bands in the Raman spectra were fitted with Lorentzian functions to obtain peak positions. XRD curves were measured on a Shimadzu XRD-6000 using Cu-Kα radiation and a scanning speed of $4^{o} \cdot min^{-1}$. WAXS measurements were carried out at NCD beamline11 (ALBA Synchrotron Light Facility, Spain) with the distance between sample and detector CCD of 20 cm. XPS measurements were performed on an ESCALab220i-XL (ThermoScientific) using a monochromatic Al-Kα X-ray source. FTIR spectra were carried out using a Thermo Nicolet NEXUS-470 FTIR instrument in the attenuated total reflection mode. UV-vis spectra were obtained using a Lambda750 spectrophotometer. Electrical conductivities were measured using a four-probe method on an electrical transport properties measurement system (Keithley 2400 multiple-function source-meter). Gravimetric electrical conductivities were obtained by dividing the inverse electrical resistance per sample length by the sample weight per sample length in the electrical conductivity direction. EMI shielding effectiveness measurements were carried out using an AV3629 vector network analyzer in the frequency range between 0.3 and 12 GHz.

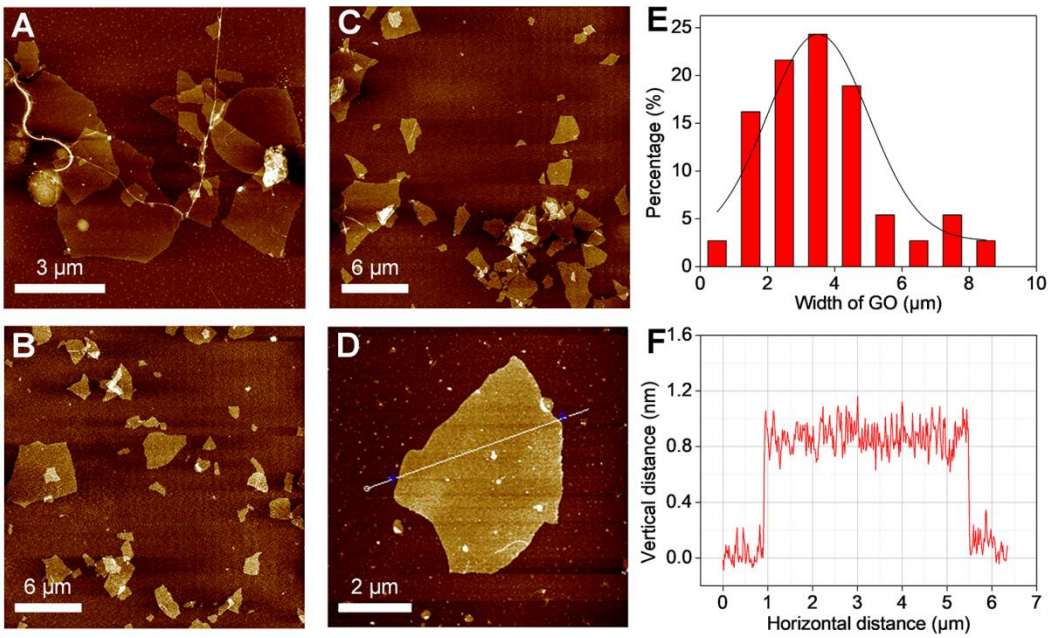

Fig. S1. Atomic force microscopy (AFM) characterization of exfoliated graphene oxide (GO) nanosheets. (A to D) AFM images of GO nanosheets. (E) The width distribution of GO nanosheets, showing that the average width of GO nanosheets is about 3.5 μm. (F) The height profile of GO nanosheets in (D), showing that the thickness of GO nanosheets is about 0.8 nm.

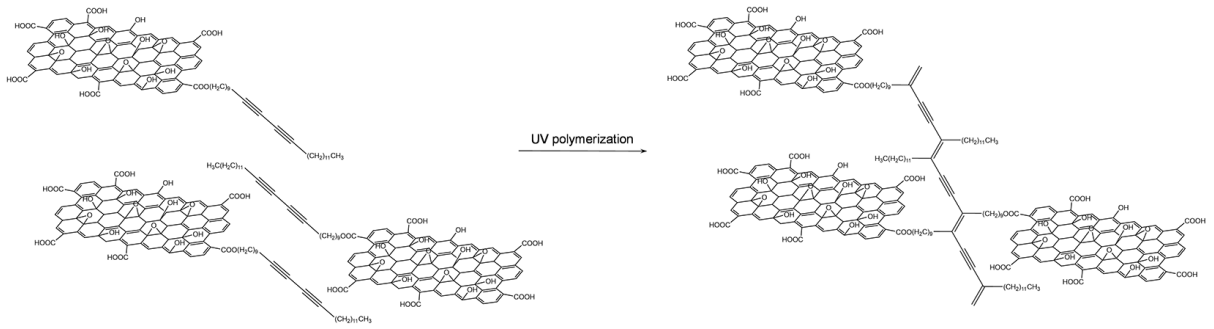

Fig. S2. (Left) Schematic illustration of an array of 10,12-pentacosadiyn-1-ol (PCO, $CH_3(CH_2)_{11}C \equiv C{-}C \equiv C(CH_2)_8CH_2OH$) molecules, whose OH groups have reacted with carboxyl groups on graphene oxide platelets. (Right) the 1,4-addition polymer formed by ultraviolet radiation of the monomer array on the left, thereby covalently connecting graphene oxide platelets. These illustrations are simplistic in that they only consider the possible function of the polydiacetylene bonding agent to reinforce the connectivity between the edges of adjacent platelets of graphene sheet stacks, and perhaps to indirectly provide enhanced bonding between graphene sheets in an individual stack. Both π-π bonding and covalent bonding between the platelet basal plane surfaces might also be especially important, and in the latter case approximately planar basal platelet planes can assist the organization of diacetylene molecules for topochemical polymerization.

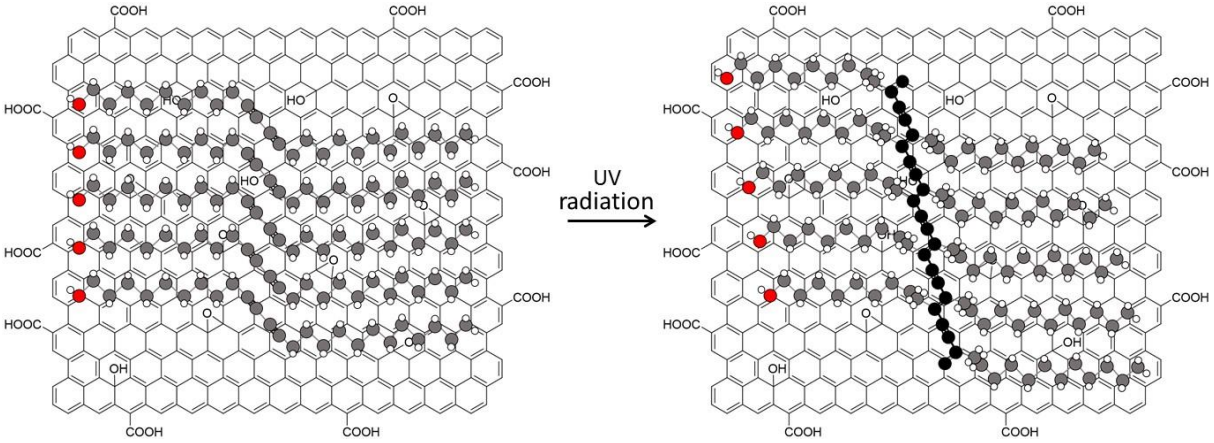

Fig. S3. Schematic illustration of the expected self-assembly of 10,12-pentacosadiyn-1-ol (PCO) molecules on the external basal-plane surface of graphene oxide platelet (left) and their polymerization by 1,4-addition polymerization to form polydiacetylene chains (right). The white spheres, red spheres, and grey spheres in the monomer array illustration represent hydrogen, oxygen, and carbon atoms, respectively. For the polymer chain, the black spheres denote carbon atoms in the polydiacetylene backbone. The observed shift in C≡C Raman vibration frequency and the observation of a long wavelength absorption due to long conjugated polydiacetylene chains confirm this polymerization. Both results were obtained for incident light normal to the sheet plane, which would maximize the intensity of both the C≡C Raman vibration and the long wavelength absorption. Based on previous scanning tunneling microscopy on graphite-substrate-supported PCO (20) and atomic force microscopy on graphite-substrate-supported 10,12-pentacosadiynoic acid (S1), arrays like pictured above are expected to be assembled in crystalline domains (having largely random orientations) on the graphene oxide (GO) surface. The carbon atoms in the polydiacetylene chain are above the graphene substrate, since these investigations show that this minimizes the atom displacements needed for 1,4-addition polymerization. While neighboring monomer arrays dimerize by hydrogen bonding on graphite, the oxygen functionalities on the GO might partially disrupt this dimerization.

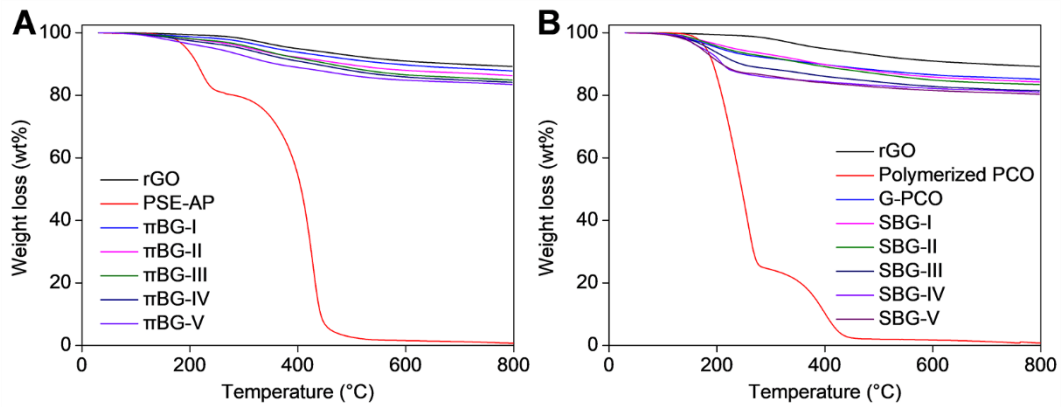

Fig. S4. Thermogravimetric analysis (TGA) curves. (A) 1-pyrenebutyric acid N-hydroxysuccinimide ester and 1-aminopyrene (PSE-AP), reduced graphene oxide (rGO), and π-bridged graphene (πBG) sheets. (B) Polymerized PCO, rGO, G-PCO, and sequentially bridged graphene (SBG) sheets. The TGA measurements were conducted under nitrogen atmosphere from room temperature to 800 ºC using a temperature increase rate of 10 ºC/min.

The weight fraction of PSE-AP in πBG sheets was estimated from the weight loss curve over the temperature range from 100 ºC to 800 ºC. The PSE-AP weight fraction (w_1) in πBG sheets is approximately given by equation 1,

$$w_1 = \frac{M_{\pi BG} - M_{rGO}}{0.992 - M_{rGO}} \quad (1)$$

where 0.992, M_{rGO} and $M_{\pi BG}$ are the fraction of weight loss for PSE-AP, rGO, and πBG sheets, respectively, between 100 ºC and 800 ºC.

The weight fraction (w_2) of PCO in sheets of G-PCO and the weight fraction (w_3) of PSE-AP in SBG sheets were analogously obtained. Since the PCO/rGO weight ratio in SBG should be the same as in G-PCO, the weight fraction (w_4) of PCO in SBG sheets should be approximately given by equation 2:

$$w_4 = (1-w_3) \times w_2 \quad (2)$$

The detailed data for PCO and PSE-AP weight percentage in G-PCO, πBG, and SBG sheets are tabulated in Table S2.

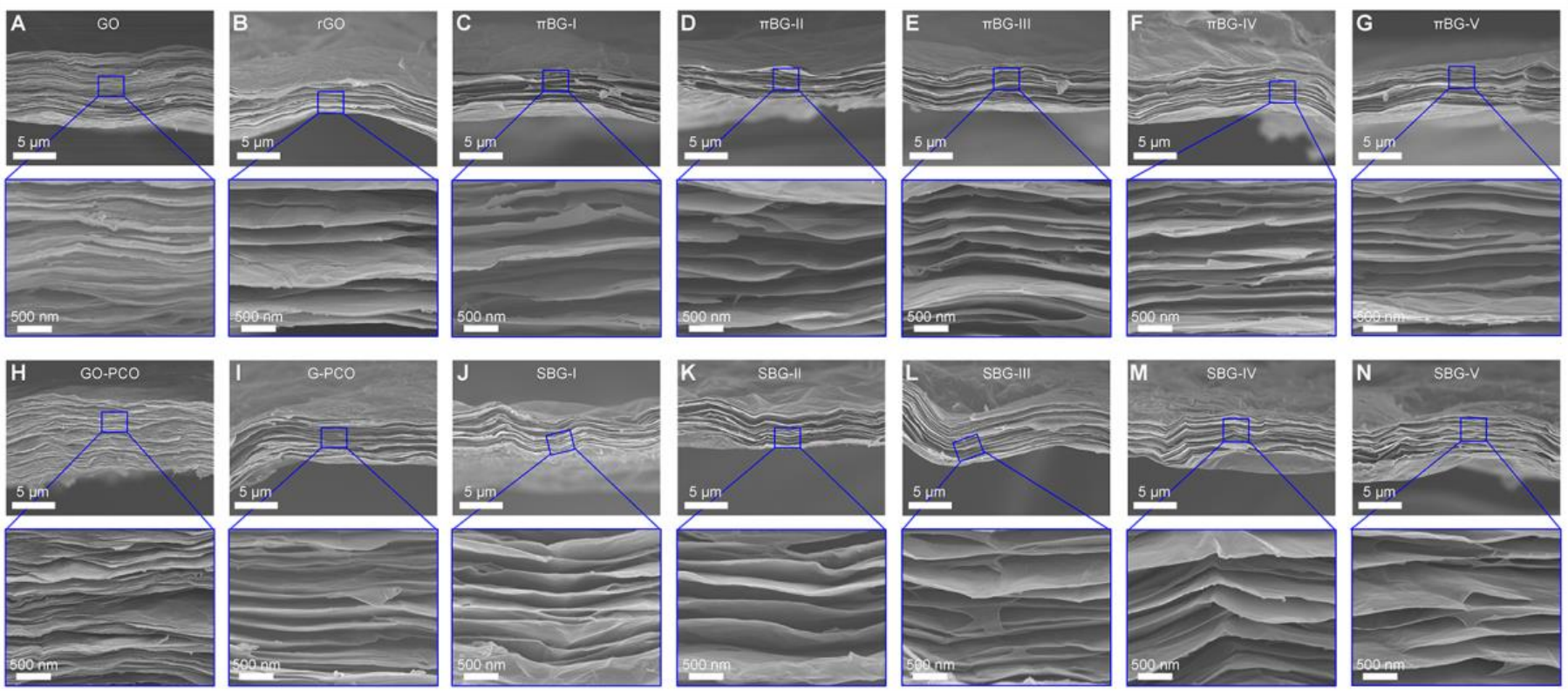

Fig. S5. Scanning electron microscope (SEM) images of sheet edges resulting from sheet fracture. (A) GO, (B) rGO, (C to G) πBG-I to πBG-V, (H) GO-PCO, (I) G-PCO, and (J to N) SBG-I to SBG-V sheets. These images show the layered structures of the sheets.

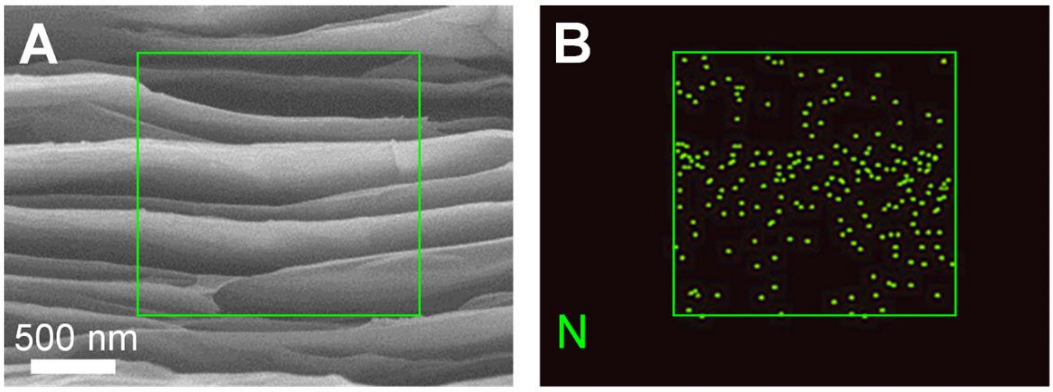

Fig. S6. (A) SEM image of cross section and (B) corresponding energy dispersive X-ray spectroscopy (EDS) mapping of nitrogen for SBG-V sheets.

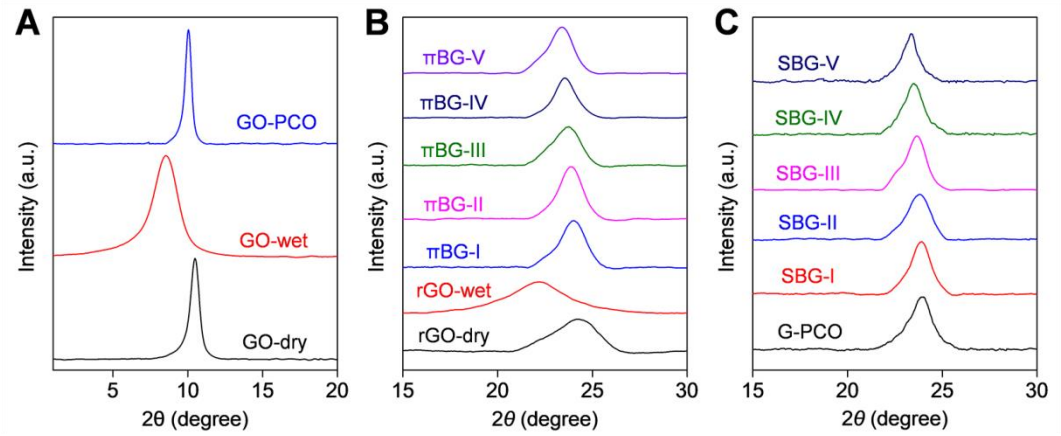

Fig. S7. X-ray diffraction (XRD) patterns using Cu-Kα radiation. (A) dry GO, wet GO (immersed in tetrahydrofuran (THF) for 1 h), and dry GO-PCO sheets. (B) dry rGO, wet rGO (immersed in N, N-dimethylformamide (DMF) for 48 h) and dry πBG sheets. (C) dry G-PCO and SBG sheets. The wet GO and rGO sheets show larger interlayer diffraction spacing than do dry GO and rGO sheets, indicating that the layers of GO and rGO sheets are separating during immersion in THF and DMF. Such separation enhances the insertion of PCO, PSE, and AP molecules into wet GO and rGO. Note that the interlayer diffraction spacings of dry G-PCO, πBG, and SBG sheets are larger than for dry rGO sheets.

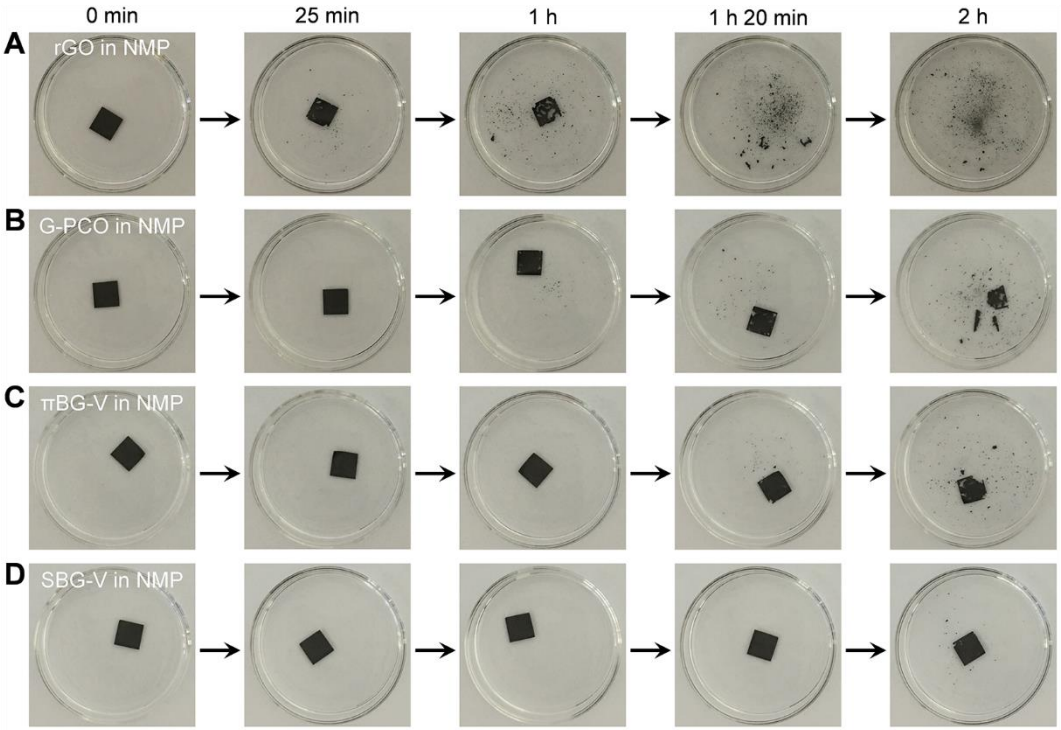

Fig. S8. Photographs of sheets during ultrasonication (using a 100 W, 40 kHz sonicator) in N-methyl-2-pyrrolidone (NMP). The (A) rGO, (B) G-PCO, (C) πBG-V, and (D) SBG-V sheets begin to disintegrate after ultrasonication for 25 min, 1 h, 1 h 20 min, and 2 h, respectively, indicating the increased resistance to disintegration of the bridged graphene sheets.

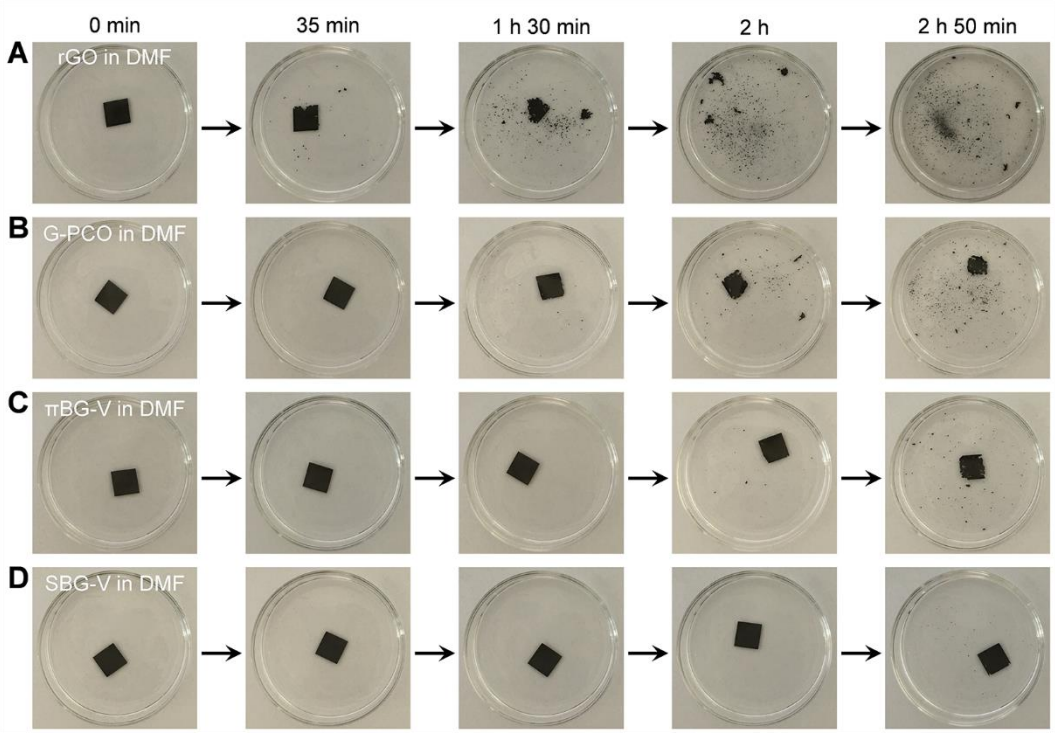

Fig. S9. Photographs of sheets during ultrasonication (using a 100 W, 40 kHz sonicator) in DMF. The (A) rGO, (B) G-PCO, (C) πBG-V, and (D) SBG-V sheets begin to disintegrate after ultrasonication for 35 min, 1 h 30 min, 2 h, and 2 h 50 min, respectively, indicating the increased resistance to disintegration of the bridged graphene sheets.

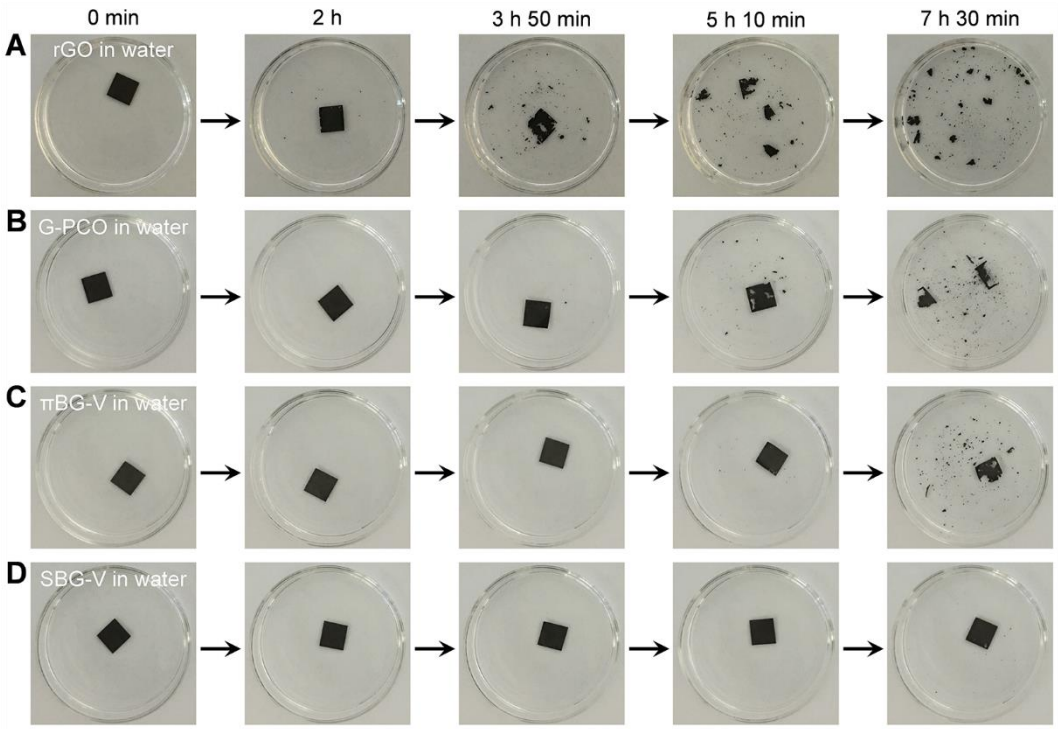

Fig. S10. Photographs of sheets during ultrasonication (using a 100 W, 40 kHz sonicator) in water. The (A) rGO, (B) G-PCO, (C) πBG-V, and (D) SBG-V sheets begin to disintegrate after ultrasonication for 2 h, 3 h 50 min, 5 h 10 min, and 7 h 30 min, respectively, indicating the increased resistance to disintegration of the bridged graphene sheets.

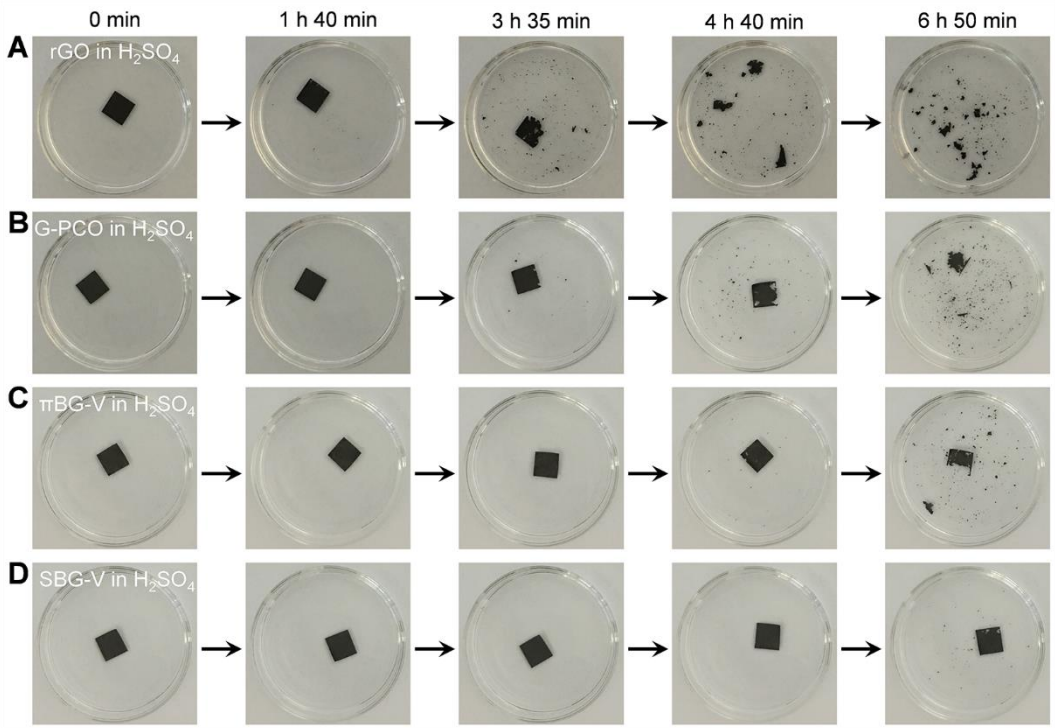

Fig. S11. Photographs of sheets during ultrasonication (using a 100 W, 40 kHz sonicator) in sulfuric acid (H_2SO_4) solution (with H^+ concentration of 8 mol·L^{-1}). The (A) rGO, (B) G-PCO, (C) πBG-V, and (D) SBG-V sheets begin to disintegrate after ultrasonication for 1 h 40 min, 3 h 35 min, 4 h 40 min, and 6 h 50 min, respectively, indicating the increased resistance to disintegration of the bridged graphene sheets.

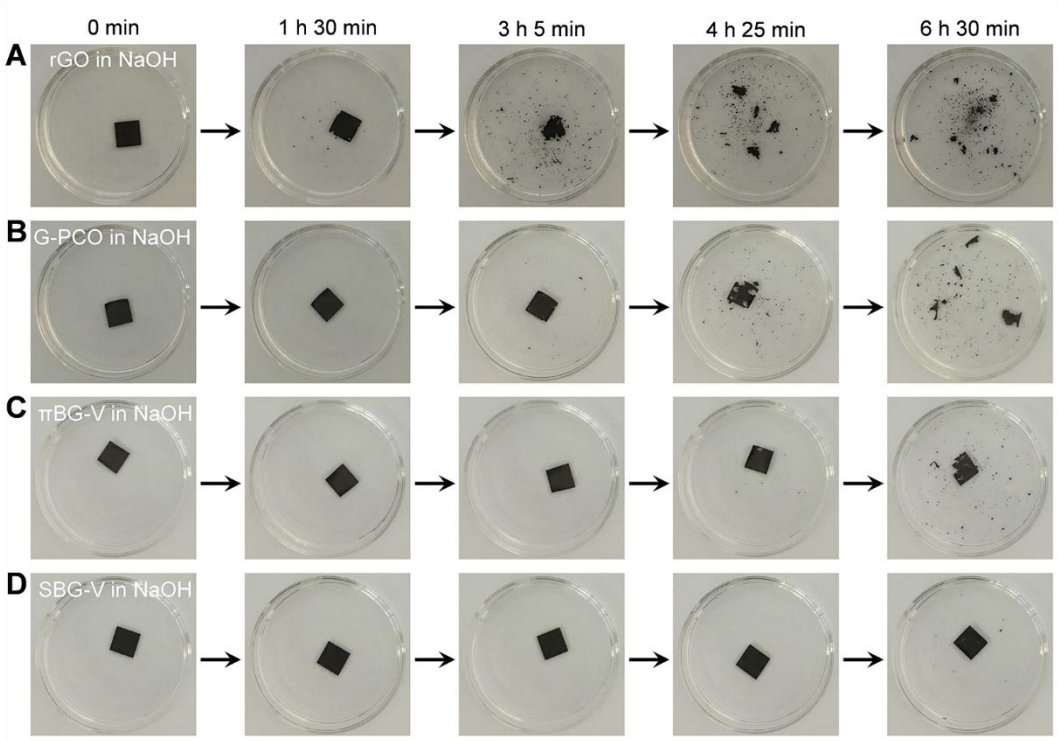

Fig. S12. Photographs of sheets during ultrasonication (using a 100 W, 40 kHz sonicator) in sodium hydroxide (NaOH) solution (with OH^- concentration of 8 $mol \cdot L^{-1}$). The (A) rGO, (B) G-PCO, (C) πBG-V, and (D) SBG-V sheets begin to disintegrate after ultrasonication for 1 h 30 min, 3 h 5 min, 4 h 25 min, and 6 h 30 min, respectively, indicating the increased resistance to disintegration of the bridged graphene sheets.

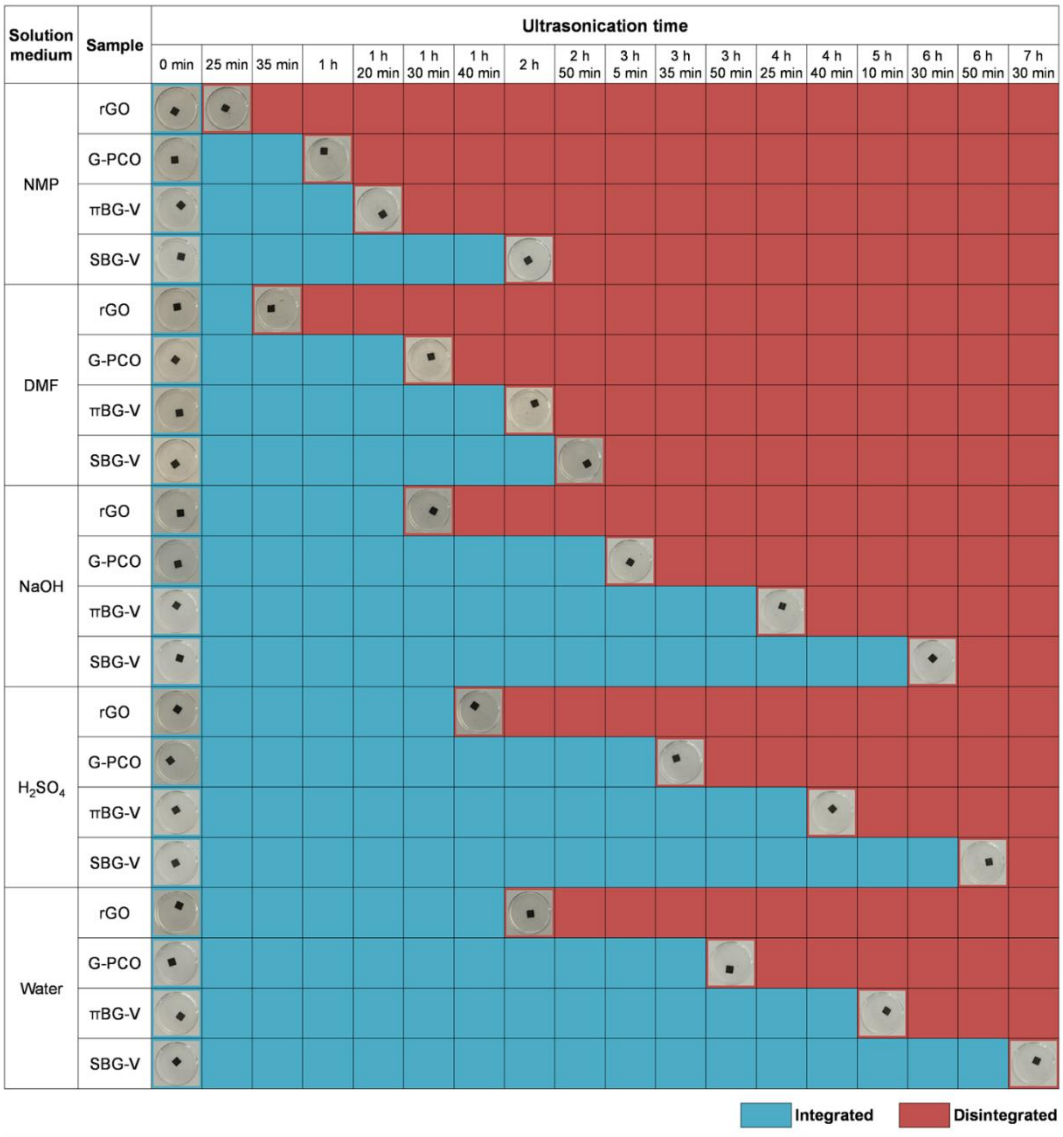

Fig. S13. The integrity of SBG sheets during ultrasonication (100 W, 40 kHz) for different times in NMP, DMF, water, H_2SO_4 (with H^+ concentration of 8 mol·L^{-1}), NaOH (with OH^- concentration of 8 mol·L^{-1}) solutions. The resistance to disintegration of sheet structure under ultrasonication in all liquids increases in going from rGO, G-PCO, and πBG-V to SBG-V.

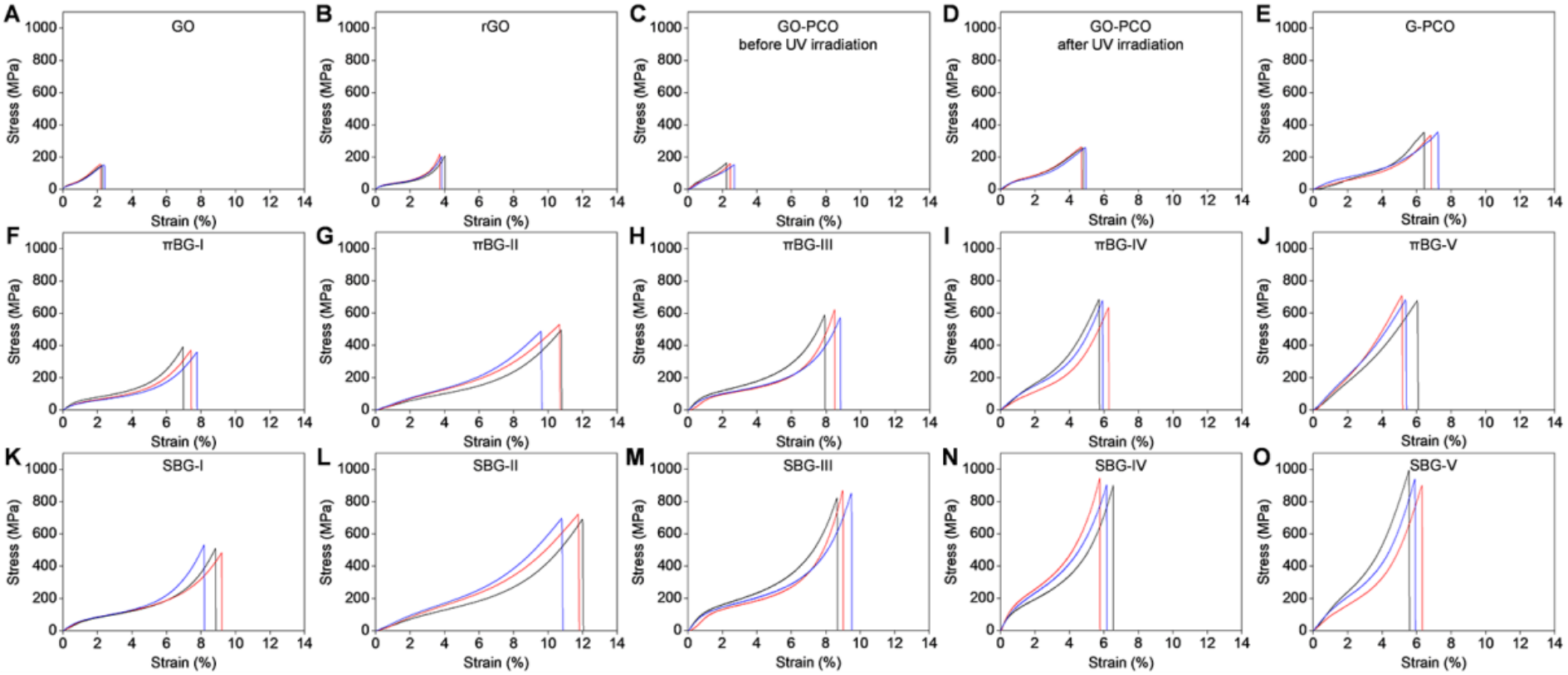

Fig. S14. Tensile stress-strain curves of sheets. (A) GO, (B) rGO, (C) GO-PCO before ultraviolet (UV) irradiation, (D) GO-PCO after UV irradiation, (E) G-PCO, (F to J) πBG-I to πBG-V, and (K to O) SBG-I to SBG-V.

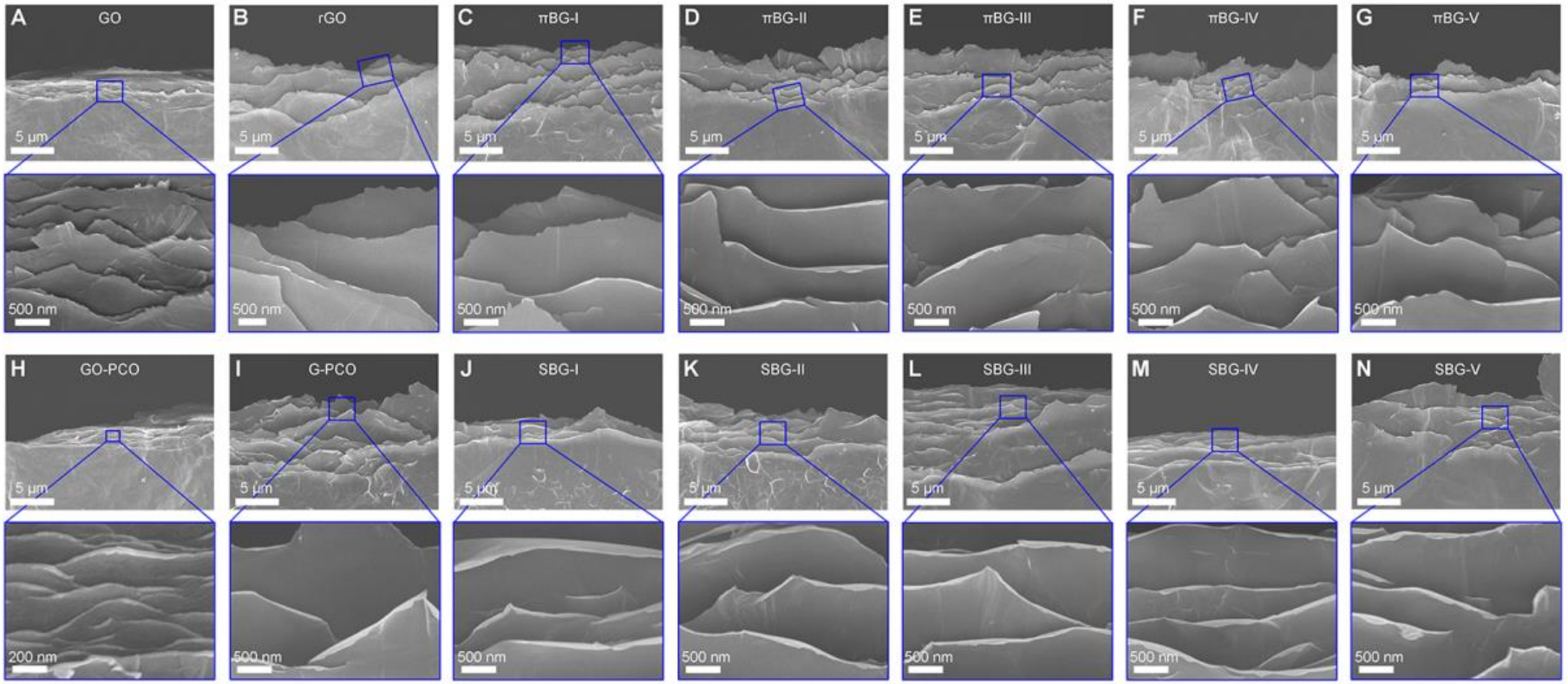

Fig. S15. Inclined-view SEM images of sheet edges resulting from sheet fracture. (A) GO, (B) rGO, (C to G) πBG-I to πBG-V, (H) GO-PCO, (I) G-PCO, and (J to N) SBG-I to SBG-V sheets. The bridged graphene sheets, including G-PCO, πBG, and SBG, curl at the fracture edge, which is not the case for the rGO sheets.

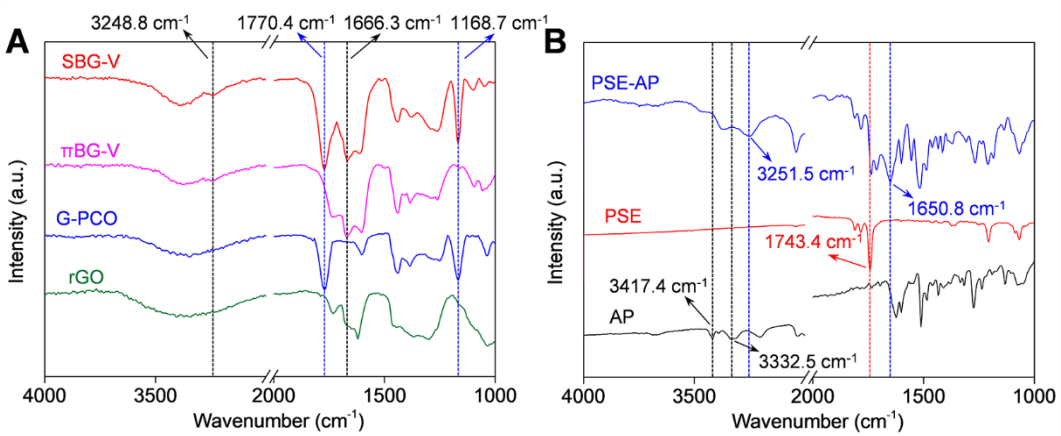

Fig. S16. Fourier transform infrared (FTIR) spectra. (A) rGO, G-PCO, πBG-V, and SBG-V sheets. (B) AP, PSE, and PSE-AP molecules. The peaks around 3251.5 cm^{-1} and 1650.8 cm^{-1} in PSE-AP correspond to the stretching vibrations of C=O and N−H, respectively, of amide groups. Thus, the peaks around 3248.8 cm^{-1} and 1666.3 cm^{-1} in πBG-V and SBG-V sheets indicate that the PSE and AP absorbed in these graphene structures have reacted to form amide linkages. The peaks around 1770.4 cm^{-1} and 1168.7 cm^{-1} in G-PCO are assigned to the stretching vibration of C=O and −C−O−C− of ester groups, demonstrating the reaction of the −OH groups of the PCO with −COOH groups of the GO nanosheets.

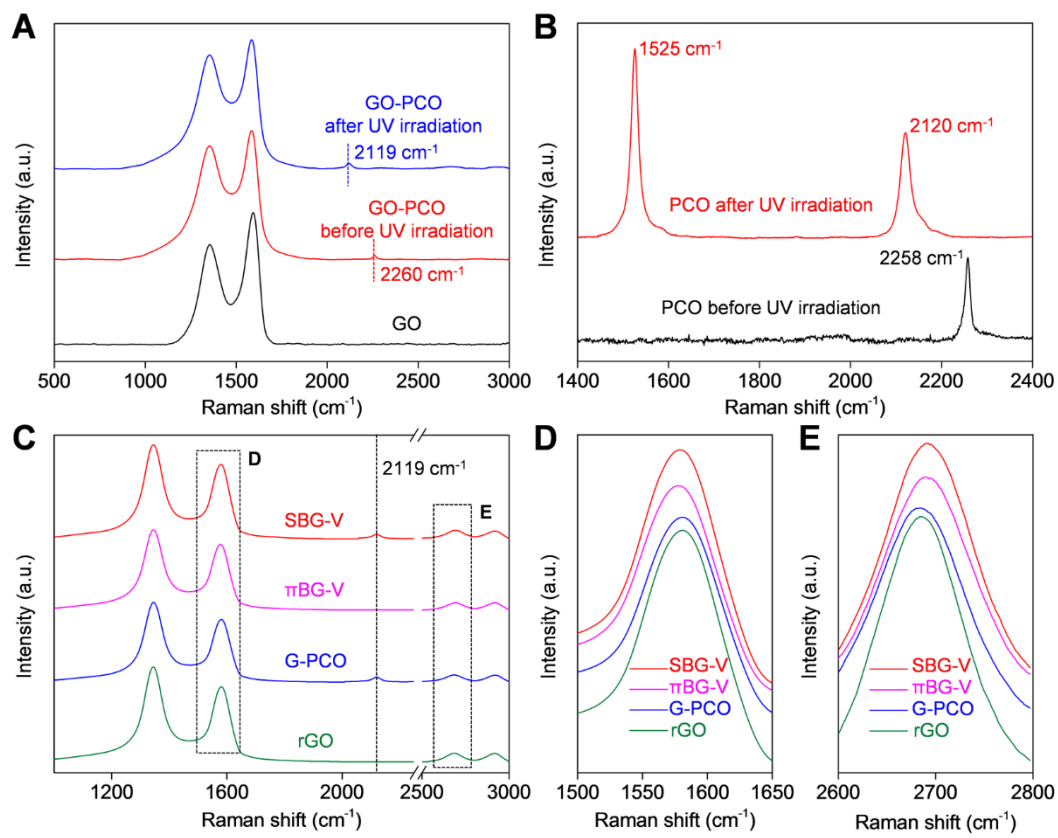

Fig. S17. Raman spectra for 633 nm excitation. (A) GO and GO-PCO sheets before and after UV irradiation (254 nm). (B) PCO before and after UV irradiation. (C) rGO, G-PCO, πBG-V, and SBG-V sheets. High resolution plots of the Raman spectra shown in (C) for Raman shift ranges of (D) 1500 to 1650 cm^{-1} and (E) 2600 to 2800 cm^{-1}. After UV irradiation, the C≡C vibration of neat PCO is down-shifted from 2258 cm^{-1} to 2120 cm^{-1} and a new peak, corresponding to the C=C vibration, appears at 1525 cm^{-1}, demonstrating the 1,4-addition polymerization of PCO. Since the PCO content in the PCO bridged sheets is relatively low, (~3.98 to ~4.21 wt%) the C=C vibration signal is so weak that it is overwhelmed by the strong G band of graphene sheets. The peak at 2119 cm^{-1} for G-PCO and SBG indicates that polymerized PCO exist in these sheets. Additionally, the G band frequency of πBG-V and SBG-V (~1578 cm^{-1}) is slightly down-shifted compared with that of rGO and G-PCO (~1581 cm^{-1}), while the 2D band frequency of πBG-V and SBG-V (~2690 cm^{-1}) is slightly up-shifted compared with that of rGO and G-PCO (~2684 cm^{-1}). The πBG-V and SBG-V sheets show similar *D/G* ratio to rGO and G-PCO sheets, respectively, as tabulated in Table S7, indicating that bridging introduces negligible disorder.

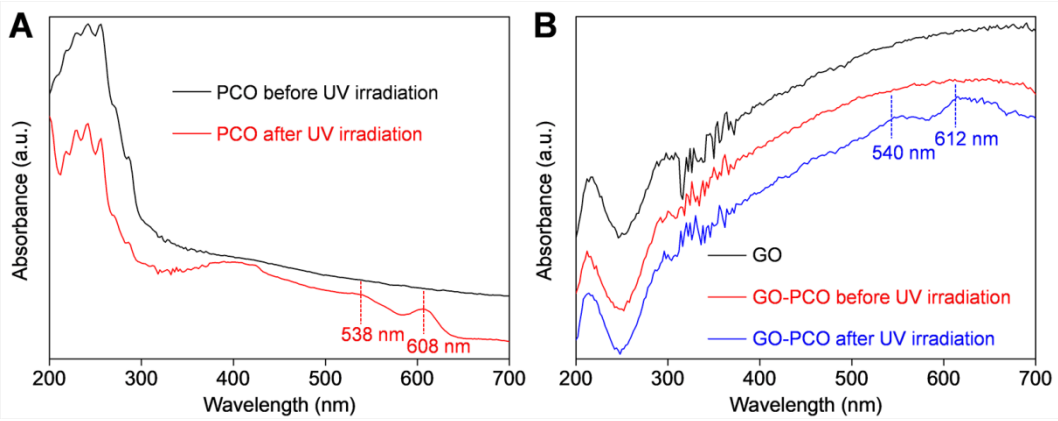

Fig. S18. Ultraviolet-visible (UV-vis) spectra. (A) PCO before and after UV irradiation. (B) GO and GO-PCO sheets before and after UV irradiation. After UV irradiation, the PCO and GO-PCO sheets show absorption peaks at 538 nm and 608 nm and at 540 nm and 612 nm, respectively, demonstrating the occurrence of the same polymerization reaction of neat PCO and GO-PCO.

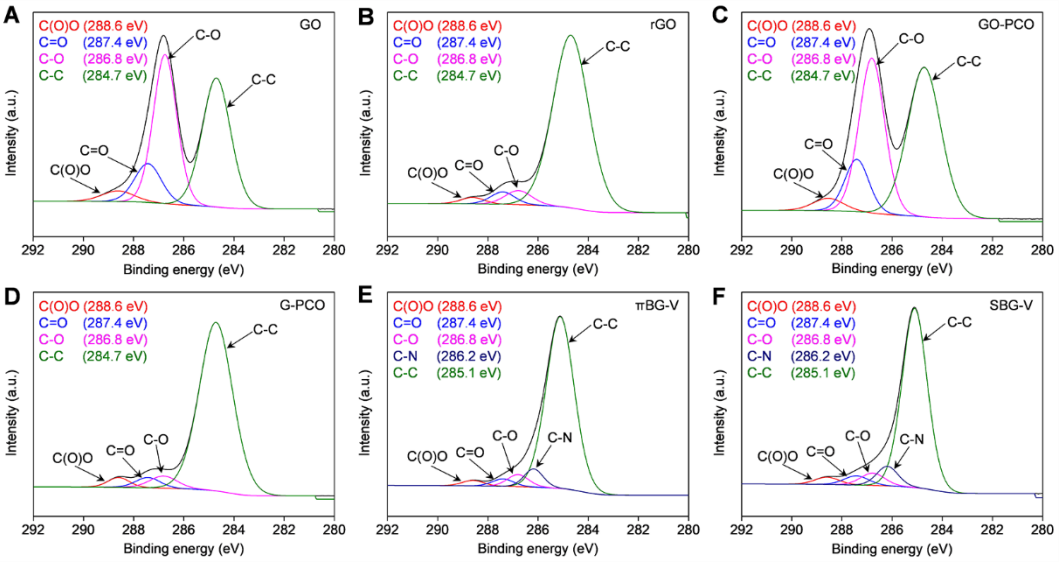

Fig. S19. X-ray photoelectron spectroscopy (XPS) for carbon. (A) GO, (B) rGO, (C) GO-PCO, (D) G-PCO, (E) πBG-V, and (F) SBG-V sheets. The broad C_{1s} peak of GO, rGO, GO-PCO, and G-PCO sheets can be fitted by four peaks at 288.6, 287.4, 286.8, and 284.7 eV, corresponding to C(O)O, C=O, C−O, and C(sp^2)−C(sp^2), respectively. The broad C_{1s} peak of πBG-V and SBG-V sheets can be fitted by five peaks at 288.6, 287.4, 286.8, 286.2, and 285.1 eV, corresponding to C(O)O, C=O, C−O, C−N, and C(sp^2)−C(sp^2), respectively. The new peak at 286.2 eV for πBG-V and SBG-V sheets is assigned to the C−N in amide groups, demonstrating the reaction between PSE and AP. Additionally, the C(sp^2)−C(sp^2) peak of πBG-V and SBG-V sheets (285.1 eV) is slightly up-shifted compared with that of GO, rGO, GO-PCO, and G-PCO sheets (284.7 eV). Furthermore, the O_{1s}/C_{1s} ratio of rGO (0.19), G-PCO (0.16), πBG-V (0.17), and SBG-V (0.16) is significantly decreased compared with that of GO (0.45) and GO-PCO (0.41), as tabulated in Table S8, indicating the substantial elimination of oxygen-containing groups of GO sheets by HI.

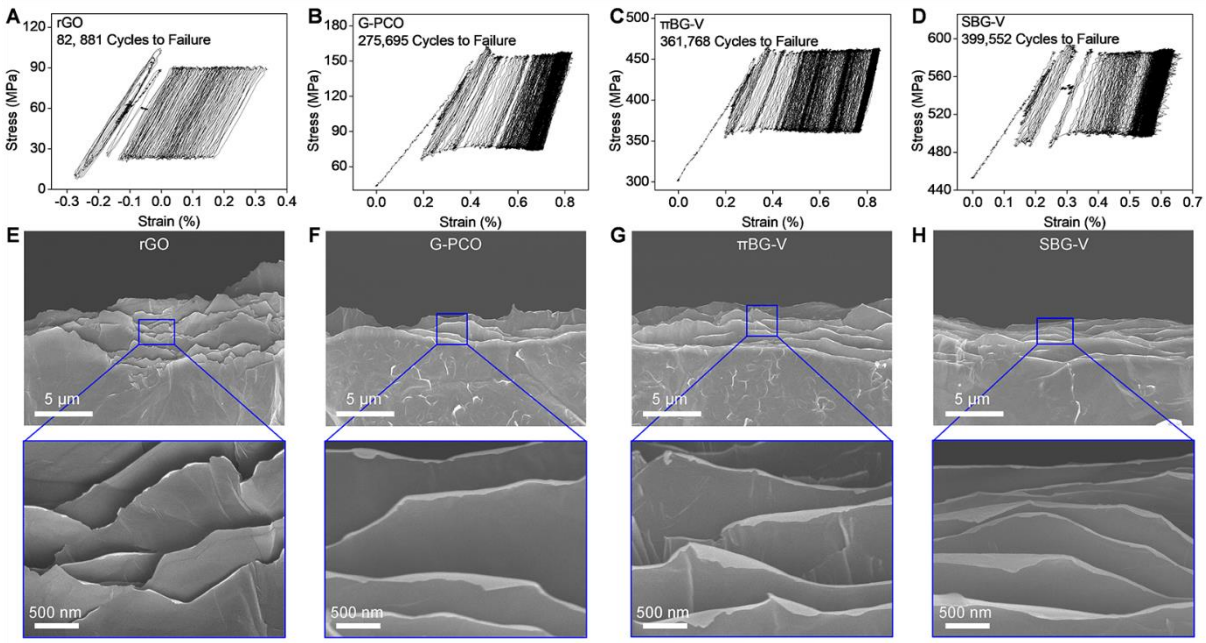

Fig. S20. Dynamic tensile stress-strain curves and corresponding fracture morphologies after tensile fatigue testing. (A and E) rGO, (B and F) G-PCO, (C and G) πBG-V, and (D and H) SBG-V sheets. The bridged graphene sheets demonstrate higher fatigue life and increased curling of fracture layer edges than rGO sheets.

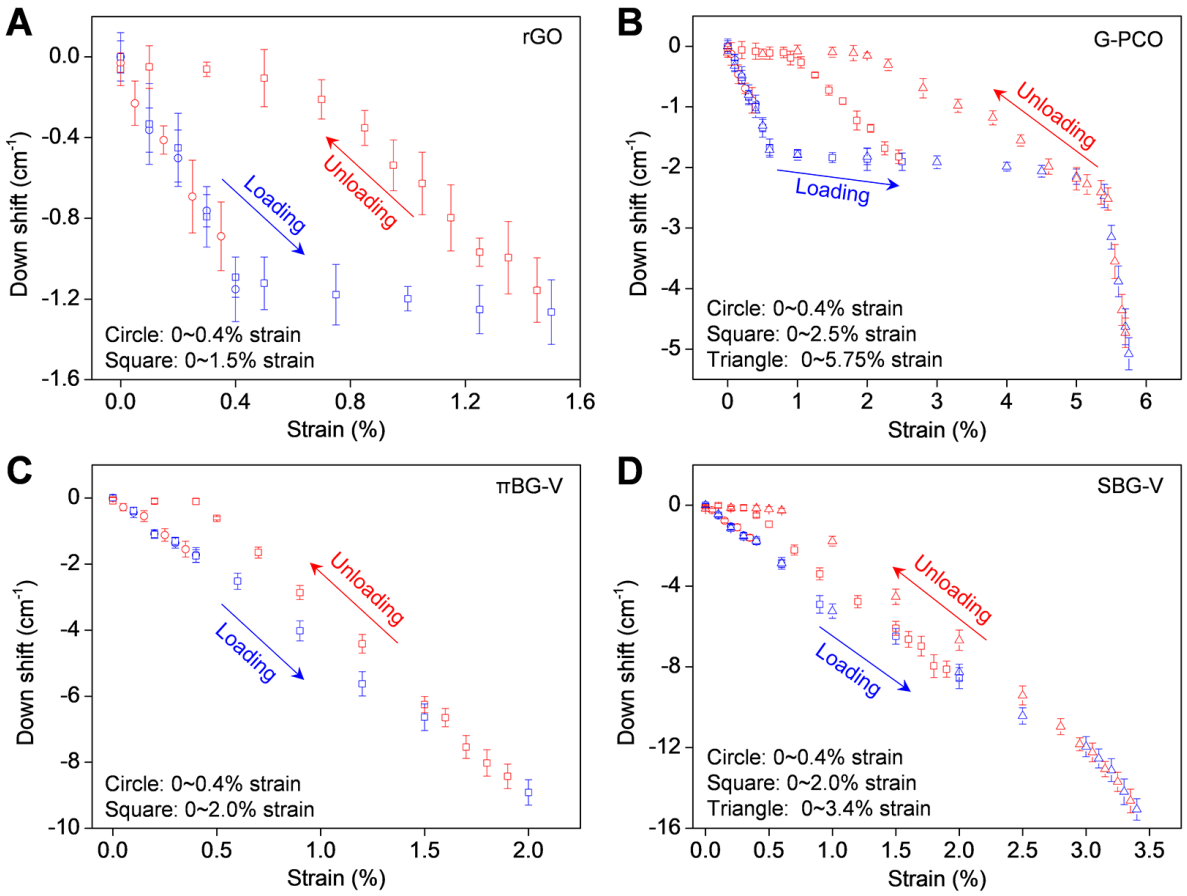

Fig. S21. Raman frequency shifts during loading/unloading processes. (A) rGO, (B) G-PCO, (C) πBG-V, and (D) SBG-V sheets. The Raman frequency shifts are reversible for these materials only when the maximum applied strain is below about 0.4%.

Table S1. The interlayer diffraction spacings of dry and wet GO, dry and wet rGO, and dry GO-PCO, G-PCO, πBG, and SBG sheets. The GO was wet by immersion in THF for 1 h and the rGO was wet by immersion in DMF for 48 h.

Sample	*d* (Å)
GO-dry	8.44
GO-wet	10.35
rGO-dry	3.66
rGO-wet	3.99
GO-PCO	8.81
G-PCO	3.72
πBG-I	3.70
πBG-II	3.72
πBG-III	3.75
πBG-IV	3.78
πBG-V	3.80
SBG-I	3.72
SBG-II	3.74
SBG-III	3.76
SBG-IV	3.79
SBG-V	3.81

Table S2. PCO and PSE-AP content of G-PCO, πBG, and SBG sheets.

Sample	PCO content (wt%) by TGA	PSE-AP content (wt%) by TGA
G-PCO	4.21	-
πBG-I	-	1.34
πBG-II	-	2.97
πBG-III	-	4.56
πBG-IV	-	5.31
πBG-V	-	5.92
SBG-I	4.17	0.94
SBG-II	4.12	2.21
SBG-III	4.03	4.32
SBG-IV	4.00	4.96
SBG-V	3.98	5.43

Table S3. The full width at half maximum (FWHM) of X-ray scattering intensity as a function of the azimuthal angle, and thereby the derived degree of graphene platelet orientation in rGO, G-PCO, πBG-V, and SBG-V sheets.

Sample	FWHM (°)	Degree of orientation (%)
rGO	41.8	76.8
G-PCO	28.7	84.1
πBG-V	25.1	86.1
SBG-V	24.5	86.4

The degree of graphene platelet orientation (Φ) was calculated using the following equation 3:

$$\Phi = \frac{180 - FWHM}{180} \times 100\% \quad (3)$$

Table S4. The tensile strength, toughness, electrical conductivity, density, gravimetric electrical conductivity, and electromagnetic interference (EMI) shielding effectiveness in the frequency range between 0.3 and 12 GHz for rGO, G-PCO, πBG-V, and SBG-V sheets. The gravimetric electrical conductivity was calculated by dividing the inverse electrical resistance per sample length by the weight per sample length in the electrical conductivity direction. Reflecting the accuracy of the density measurements for these thin sheets, nearly the same gravimetric electrical conductivity was obtained by dividing the electrical conductivity by the sample density.

Sample	Tensile strength (MPa)	Toughness (MJ/m^3)	Electrical conductivity ($S \cdot cm^{-1}$)	Density ($g \cdot cm^{-3}$)	Gravimetric electrical conductivity ($S \cdot cm^2 \cdot g^{-1}$)	EMI shielding effectiveness in the frequency range between 0.3 and 12 GHz (dB)
rGO	209.7 ± 8.0	2.6 ± 0.1	186.8 ± 16.9	2.01	92.9 ± 8.4	~11
G-PCO	348.5 ± 12.0	8.5 ± 1.3	357.2 ± 18.6	2.03	176.0 ± 9.2	~16
πBG-V	688.5 ± 17.0	16.6 ± 1.2	440.5 ± 21.3	2.04	215.9 ± 10.4	~21
SBG-V	944.5 ± 46.6	20.6 ± 1.0	512.3 ± 24.5	2.07	247.5 ± 11.8	~27

Table S5. The thickness and mechanical properties of GO, rGO, G-PCO, πBG, and SBG sheets and the thickness and mechanical properties of GO-PCO sheets before and after UV irradiation.

Sample	Thickness (μm)	Young's modulus (GPa)	Tensile strength (MPa)	Toughness (MJ/m^3)	Strain to failure (%)
GO	7.6 ± 0.4	17.1 ± 1.1	151.3 ± 3.2	1.6 ± 0.1	2.3 ± 0.1
rGO	3.4 ± 0.2	8.0 ± 0.9	209.7 ± 8.0	2.6 ± 0.1	3.9 ± 0.2
GO-PCO before UV irradiation	8.2 ± 0.3	7.8 ± 1.2	157.2 ± 6.1	1.8 ± 0.1	2.4 ± 0.2
GO-PCO after UV irradiation	8.0 ± 0.4	7.6 ± 0.5	258.7 ± 2.8	5.5 ± 0.1	4.8 ± 0.1
G-PCO	3.8 ± 0.1	5.3 ± 0.6	348.5 ± 12.0	8.5 ± 1.3	6.8 ± 0.4
πBG-I	3.3 ± 0.3	6.9 ± 1.2	372.7 ± 16.4	9.4 ± 0.2	7.4 ± 0.4
πBG-II	2.7 ± 0.2	5.8 ± 0.6	502.4 ± 22.0	19.1 ± 1.9	10.3 ± 0.7
πBG-III	3.4 ± 0.2	10.6 ± 1.7	593.9 ± 24.5	16.5 ± 0.7	8.4 ± 0.5
πBG-IV	4.1 ± 0.2	9.1 ± 1.1	664.8 ± 27.0	14.6 ± 0.8	6.0 ± 0.3
πBG-V	3.7 ± 0.2	11.1 ± 1.2	688.5 ± 17.0	16.6 ± 1.2	5.5 ± 0.5
SBG-I	3.2 ± 0.1	7.0 ± 0.4	508.2 ± 24.3	14.9 ± 0.9	8.7 ± 0.5
SBG-II	3.2 ± 0.1	5.7 ± 0.5	702.7 ± 16.1	29.8 ± 2.1	11.5 ± 0.6
SBG-III	3.8 ± 0.2	13.3 ± 1.6	847.6 ± 23.0	25.4 ± 2.0	9.1 ± 0.4
SBG-IV	3.7 ± 0.2	18.5 ± 1.6	916.0 ± 25.0	22.1 ± 0.4	6.2 ± 0.4
SBG-V	3.3 ± 0.2	15.6 ± 1.0	944.5 ± 46.6	20.6 ± 1.0	5.9 ± 0.4

Table S6. The mechanical properties of SBG-V sheets, and other materials having high strengths in all sheet plane directions, including graphene sheet composites, carbon nanotube sheet composites, and carbon fiber composites.

Number	Materials	Tensile strength (MPa)	Toughness (MJ/m^3)	Reference
1	**Wet-spun rGO sheet**	172.2	0.8	(13)
2	**Collapsed graphene sheet**	22.5	1.7	(10)
3	**Debris-free graphene sheet**	60.0	4.8	(11)
4	**g-rGO**	614.0	14.9	(12)
5	**rGO-SL**	300.0	2.8	(34)
6	**rGO-PVA**	188.9	2.5	(29)
7	**rGO-PAA**	309.6	8.9	(36)
8	**rGO-PDA**	204.9	4.0	(24)
9	**rGO-PCDO**	129.6	3.9	(14)
10	**rGO-CS**	526.7	17.7	(27)
11	**rGO-PAPB**	382.0	7.5	(32)
12	**rGO-CNC**	655.0	1.8	(31)
13	**rGO-MoS_2-TPU**	235.0	6.9	(26)
14	**rGO-DWNT-PCDO**	374.1	9.2	(25)
15	**rGO-MMT-PVA**	356.0	7.5	(35)
16	**rGO-WS_2-PCDO**	413.6	17.7	(28)
17	**ai-rGO-CNC**	765.0	15.6	(30)
18	**T300-3K-PW/F655 BMI**	665.0	3.6	(38)
19	**AS4C-3K-PW/M65 BMI**	841.0	6.3	(38)
20	**AS4-3K-PW/8552 Epoxy**	793.0	4.8	(38)
21	**AS4-3K-5HS/8552 Epoxy**	800.0	4.8	(38)

22	**IM7-6K-PW/8552 Epoxy**	945.0	5.6	(38)
23	**IM7-6K-8HS/8552 Epoxy**	959.0	5.7	(38)
24	**T300-3K-8HS/F593 Epoxy**	563.0	2.8	(38)
25	**T300-3K-PW/F593 Epoxy**	637.0	3.6	(38)
26	**AS4C-6K-Twill/M21 Epoxy**	885.0	5.8	(38)
27	**T700-12K-Twill/M47 Epoxy**	900.0	6.6	(38)
28	**AS4-3K-Twill/M47 Epoxy**	930.0	6.3	(38)
29	**CHS-6K-Twill/M81 Epoxy**	870.0	5.6	(38)
30	**AS4C-3K-5HS/M92 Epoxy**	782.0	6.1	(38)
31	**AS4C-3K-PW/M92 Epoxy**	687.0	4.7	(38)
32	**SWNT-PEI-PAA**	175.0	0.9	(6)
33	**SWNT-PS**	51.0	0.4	(41)
34	**SWNT-Epoxy**	550.0	11.0	(43)
35	**MWNT-PEI-PAA**	165.0	4.6	(42)
36	**FDWCNT-Epoxy**	450.0	9.6	(40)
37	**MWNT-BMI**	620.0	7.8	(39)
38	**SBG-V**	944.5	20.6	This work

Table S7. The *D/G* Raman intensity ratios for GO, rGO, GO-PCO, G-PCO, πBG-V, and SBG-V sheets using 633 nm excitation.

Sample	*D/G*
GO	1.15
rGO	1.61
GO-PCO	1.37
G-PCO	1.69
πBG-V	1.62
SBG-V	1.69

Table S8. The O_{1s}/C_{1s} atomic ratios for GO, rGO, GO-PCO, G-PCO, πBG-V, and SBG-V sheets.

Sample	O_{1s}/C_{1s} (atomic ratios)
GO	0.45
rGO	0.19
GO-PCO	0.41
G-PCO	0.16
πBG-V	0.17
SBG-V	0.16

References

S1. Okawa Y, Takajo D, Tsukamoto S, Hasegawa T, Aono M (2008) Atomic force microscopy and theoretical investigation of the lifted-up conformation of polydiacetylene on a graphite substrate. *Soft Matter* 4:1041-1047.